J. Fluid Mech. (1992), *vol.* 245, *pp.* 137–154

A numerical investigation of non-spherical rebounding bubbles

By J. P. BEST[1] AND A. KUCERA[2]

[1] Materials Research Laboratory – DSTO, PO Box 50, Melbourne, 3032, Australia

[2] Department of Mathematics, Australian Defence Force Academy, Campbell, ACT, 2600, Australia

(Received 27 June 1991 and in revised form 18 February 1992)

The motion of buoyant transient cavities with non-condensible contents is investigated numerically using a boundary-integral method. The bubble contents are described by an adiabatic gas law. Motion is considered in the neighbourhood of a rigid boundary, in an axisymmetric geometry. We investigate whether the non-condensible contents will resist the formation of jets. It is found that jets form upon collapse and, in general, completely penetrate the bubble before it rebounds, but circumstances are identified under which the non-spherical bubble will rebound prior to this occurrence. In these cases the bulk of the jet growth occurs upon rebound. Furthermore, the interaction between the buoyancy force causing jet formation upwards, and the Bjerknes attraction of the rigid boundary causing jet formation towards it, is investigated and general principles discussed which allow the behaviour to be interpreted. The concept of the Kelvin impulse is utilized.

1. Introduction

The collapse of transient cavities adjacent to structures is a problem of considerable engineering significance. The collapse of a cavitation bubble near to a rigid boundary is accompanied by the formation of a high-speed liquid jet, directed towards the boundary. Experimental investigations (Tomita & Shima 1986) have demonstrated the pitting of the surface caused by this phenomenon. A problem of larger scale, yet similar fluid mechanics, is that of the collapse of the bubble produced by an underwater explosion, again with characteristic high-speed liquid jets formed upon collapse (Wilkerson 1989).

The boundary-integral method has become a popular and successful technique for computing the motion of cavities when the fluid is considered as inviscid and incompressible, and the flow induced by the bubble's motion as irrotational (Guerri, Lucca & Prosperetti 1981; Blake, Taib & Doherty 1986, 1987; Chahine & Perdue 1988; Wilkerson 1989). The majority of these studies, however, have assumed that the bubble contains only the liquid vapour and that it exerts a constant pressure throughout the lifetime of the bubble. Experimental evidence indicates that this is not quite an appropriate description. Many high-speed photographic records of bubble collapse (Benjamin & Ellis 1966; Lauterborn & Bolle 1975; Vogel, Lauterborn & Timm 1989) reveal that the bubble rebounds and undergoes several oscillations, although in a form perturbed from a spherical shape. That this behaviour should be observed may be explained by supposing that the later stages of the collapse proceed so quickly that the liquid vapour does not completely condense. The rapid decrease in bubble volume causes the compression of this non-condensing gas and the resultant

high pressure causes the bubble to rebound. It is clear in the example of underwater explosion bubbles that this should occur, as the bubble contents consist primarily of the remnants of the detonation which are non-condensible. Indeed, much attention during WWII was focused upon the emission of finite-amplitude pressure pulses by the rebound of explosion bubbles, and their possible action as a secondary damage-causing agent.

The presence of non-condensible bubble contents prompts the interesting speculation that the high pressure developed within the bubble upon collapse may be sufficient to arrest jet formation. In this paper we address this question by undertaking a numerical investigation of transient cavity motion in which there is a quantity of non-condensible gas within the bubble. We utilize a boundary-integral method and employ an adiabatic gas law description of the bubble contents. Motion is considered in an axisymmetric geometry, and buoyancy forces and the presence of a nearby rigid boundary are the influences that perturb the bubble from spherical shape. It is found that the presence of a non-condensible gas will not arrest the formation of a jet, only delay it, with examples presented where the bulk of the growth of the jet occurs upon rebound.

We further investigate the interaction between the perturbing agents of buoyancy and nearby boundaries. It is established that buoyancy induces jet formation directed in opposition to the gravitational acceleration, whereas the Bjerknes attraction of a rigid boundary causes jet formation directed towards it. By considering axisymmetric motion above and below a rigid boundary we may investigate how these effects positively and negatively couple and deduce qualitative principles with which to interpret the observed behaviour. This endeavour is assisted considerably by exploiting the Kelvin impulse and this concept is discussed.

2. The mathematical description

Suppose that a bubble undergoes some motion in a fluid and denote the domain occupied by the fluid as Ω, with $\partial\Omega$ its boundary. The bubble surface, S, is a subset of $\partial\Omega$ and in the case where motion occurs in an infinite fluid $S \equiv \partial\Omega$. We denote by $\boldsymbol{n}$ the normal to $\partial\Omega$, exterior to Ω. We allow for the presence of a uniform gravitational field and choose a Cartesian set of axes, defined by the orthonormal basis $\boldsymbol{e}_x, \boldsymbol{e}_y, \boldsymbol{e}_z$, such that the gravitational acceleration is $\boldsymbol{g} = -g\boldsymbol{e}_z$.

We describe the fluid as inviscid and incompressible and the flow induced by the bubble's motion as irrotational. A velocity potential, ϕ, is introduced so that the fluid velocity, $\boldsymbol{u}$, is given as the gradient of the potential which itself satisfies Laplace's equation in Ω:

$$\boldsymbol{u} = \nabla\phi, \quad \nabla^2\phi = 0. \tag{1}$$

On $\partial\Omega$ appropriate boundary conditions are applied. There is no flow normal to a rigid boundary and at free boundaries the potential is assumed to be known. For most of the lifetime of a cavitation or explosion bubble the curvature of the bubble surface is insufficient to cause any appreciable effect upon the dynamics of the bubble via the action of surface tension. Hence surface tension is neglected in this investigation. Computations including this effect have been performed and the reader is referred to the work of Chahine & Perdue (1988) and Chahine (1990) for details.

We employ an elementary description of the bubble contents. Studies of cavitation bubble dynamics have assumed that the bubble contents consist of the liquid vapour,

and that it exerts a constant pressure, p_c, throughout the lifetime of the bubble. An explosion bubble contains the non-condensible remnants of a detonation, and there is evidence to suggest that cavitation bubbles would be better described by taking account of some non-condensible contents. We suppose that we can describe this non-condensing gas as ideal, and that on the timescale of the bubble oscillation there is negligible heat exchange with the surrounding fluid, so that the expansions and compressions of this gas are adiabatic. Hence we write the pressure, p_b, exerted by the bubble contents as a function of the volume, V, via

$$p_b = p_c + p_0(V_0/V)^\lambda, \tag{2}$$

where the subscript 0 denotes initial quantities, λ is the ratio of specific heats and we have allowed for the presence of some liquid vapour within the bubble. For the products of various explosives λ is empirically determined. In this investigation we take $\lambda = 1.4$. As a matter of terminology, in what follows we shall refer to cavitation bubble motion that described by a constant pressure within the bubble, and to explosion bubble motion that described by (2).

Lengths are scaled with respect to the maximum bubble radius, R_m, time with respect to $R_m(\rho/\Delta p)^{\frac{1}{2}}$ and $\Delta p = p_\infty - p_c$ is the pressure scale, where ρ is the density and p_∞ is the hydrostatic pressure at the depth at which inception of the motion occurs. The Bernoulli equation is used to determine the evolution of free surfaces. The bubble surface, S, is a free surface and evaluating the Bernoulli equation here yields

$$\partial\phi/\partial t + \tfrac{1}{2}|\nabla\phi|^2 + \alpha(V_0/V)^\lambda + \delta^2(z - z_0) - 1 = 0, \tag{3}$$

where

$$\delta = (\rho g R_m/\Delta p)^{\frac{1}{2}} \tag{4}$$

is the buoyancy parameter and we call

$$\alpha = p_0/\Delta p \tag{5}$$

the strength parameter. Physically δ corresponds to the ratio of the bubble half-life to the time it would take a bubble of radius R_m to rise the order of one radius from rest due to buoyancy forces. It thus provides a measure of the strength of the buoyancy force. The strength parameter provides some measure of the magnitude of the initial partial pressure exerted by the non-condensible bubble contents. In the case of an underwater explosion bubble this pressure is high and drives the oscillation of the bubble. For motion near to a horizontal rigid boundary it is convenient at this point to introduce γ as

$$\gamma = \xi_0/R_m, \tag{6}$$

where ξ_0 is the distance away from the boundary at which inception of the motion occurs. γ characterizes the Bjerknes attraction of the boundary and takes on positive or negative values according to whether the motion occurs above or below the boundary.

We complete the description of the model with the provision of initial conditions. In the study of cavitation-bubble dynamics it is assumed that the Rayleigh equation (Rayleigh 1917) describing motion in an infinite fluid provides an approximate description of the earliest motion of the bubble. This is not unreasonable as during short intervals when the bubble is very small, the buoyancy force is negligible and the presence of nearby boundaries is little felt. Thus the bubble is initially supposed to be spherical and of some initial radius, R_0. The corresponding initial time, t_0, and

potential on the bubble surface, ϕ_0, are determined from the Rayleigh equation. In accord with Blake *et al.* (1986) the initial conditions for a cavitation bubble are

$$R_0 = 0.1, \quad \phi_0 = -2.5806976, \quad t_0 = 0.0015527. \tag{7}$$

The bubble surface at this time is moving outwards with a radial velocity of 25.806976.

In the explosion bubble example, the presence of the non-condensible gas provides a much greater freedom in the choice of initial conditions. At the initial small radius, R_0, the non-condensible gas is highly compressed and the large initial partial pressure, p_0, drives the motion, in addition to any initial radial velocity imposed upon the system. We thus have the option of choosing a multitude of combinations of initial pressure and radial velocity, the assumption that the bubble is initially spherical being retained. This freedom of choice is superfluous due to the relative unimportance of buoyancy and boundary effects during the early phases of the motion. Consider the equation describing the motion in an infinite fluid of a bubble whose contents are described by (2). It is

$$R\ddot{R} + \tfrac{3}{2}\dot{R}^2 = \alpha(R_0/R)^{3\lambda} - 1, \tag{8}$$

where the above time- and lengthscales have been employed. The motion is purely radial and R denotes the radius. Equation (8) describes oscillatory motion so that given an initial non-zero radial velocity we may integrate (8) backwards in time to obtain a new initial radius and pressure (new value of α) corresponding to a zero initial radial velocity. For all except very small-amplitude radial oscillations the time over which this backwards integration must take place is negligible compared to the period of the oscillation, so that the motion over this time is little influenced by the presence of boundaries or the buoyancy force.

Thus we suppose that the initial radial velocity of the explosion bubble is zero, with the motion driven from rest by the very high initial partial pressure p_0. The initial potential on the bubble surface is equal to zero. The initial radius is chosen such that the maximum radius to which the bubble would expand in an infinite fluid is equal to one and this value is obtained from the solution of (8).

3. The boundary-integral method

We utilise the boundary-integral method of Kucera (1992) (following Blake *et al.* 1986) to investigate the motion of explosion bubbles, whose internal pressure is a function of the bubble volume. Application of Green's theorem yields the solution of Laplace's equation in the domain Ω as

$$c(\boldsymbol{p})\,\phi(\boldsymbol{p}) = \int_{\partial\Omega} \left(\frac{\partial\phi}{\partial n}(\boldsymbol{q})\, G(\boldsymbol{p},\boldsymbol{q}) - \phi(\boldsymbol{q}) \frac{\partial G}{\partial n}(\boldsymbol{p},\boldsymbol{q}) \right) \mathrm{d}S(\boldsymbol{q}), \tag{9}$$

with

$$c(\boldsymbol{p}) = \begin{cases} 2\pi, & \boldsymbol{p} \in \partial\Omega, \\ 4\pi, & \boldsymbol{p} \in \Omega \backslash \partial\Omega \end{cases} \quad \text{and} \quad G(\boldsymbol{p},\boldsymbol{q}) = \frac{1}{|\boldsymbol{p}-\boldsymbol{q}|}. \tag{10}$$

The point $\boldsymbol{p}$ is somewhere in the flow domain and $\partial/\partial n \equiv \boldsymbol{n}\cdot\nabla$ is the normal derivative at the boundary. $\Omega\backslash\partial\Omega$ denotes the complement of $\partial\Omega$ in Ω and $\partial\Omega$ is supposed to be everywhere smooth. For motion in the neighbourhood of a rigid boundary an image term is added to the Green's function so that $\partial\Omega$ may be considered as the bubble surface alone, with the rigid boundary condition implicitly satisfied.

The principle of the method is as follows. At some time t, S and ϕ on S are known. Equation (9) is then a Fredholm integral equation of the first kind for the normal fluid velocity, $\partial\phi/\partial n$, at the bubble surface. Solution for this quantity allows the fluid velocity, $\boldsymbol{u}$, at the bubble surface to be determined. Letting $\boldsymbol{X}$ denote the position vector of some point on the bubble surface we may then integrate the equation

$$\mathrm{d}\boldsymbol{X}/\mathrm{d}t = \boldsymbol{u}, \tag{11}$$

describing the motion of points on the bubble surface in the Lagrangian sense. The rate of change of ϕ following some fluid element at S is

$$\mathrm{d}\phi/\mathrm{d}t = \partial\phi/\partial t + |\nabla\phi|^2 = \tfrac{1}{2}|\nabla\phi|^2 - \alpha(V_0/V)^\lambda - \delta^2(z-z_0) + 1, \tag{12}$$

$\partial\phi/\partial t$ having been eliminated using the Bernoulli equation. This equation is integrated simultaneously with (11), giving ϕ on S as a function of time.

To solve (9) we employ a collocation method in an axisymmetric geometry. A set of $n+1$ nodes are chosen on the surface of the bubble, with the assumption of axisymmetry necessitating only the description of a curve in two dimensions. The surface of the bubble is represented by a cubic spline, constrained to pass through the node points. The spline parameter is the arclength, s, along the curve that is the bubble surface. If r and z respectively denote the radial and vertical coordinates of points on the bubble surface then these are locally cubic functions of s. The arclength and spline coefficients are determined iteratively using the technique developed by Kucera (1992) that yields the exact arclength along the curve. A consequence of this parameterization is that the spline functions satisfy

$$(\mathrm{d}r/\mathrm{d}s)^2 + (\mathrm{d}z/\mathrm{d}s)^2 = 1. \tag{13}$$

In the computations presented here, 33 node points were used to define the bubble surface. We represent the value of ϕ over S using a cubic spline, parameterized with respect to s. The value of $\partial\phi/\partial n$ at node i is denoted by ψ_i, and these quantities are unknown. If we represent $\partial\phi/\partial n$ on S linearly with respect to s then collocation of (9) at the nodes yields a set of linear equations for the ψ_i that are solved by standard techniques. In carrying out the surface integral of (9) the integration over the azimuthal angle is performed analytically, yielding expressions involving elliptic integrals of the first and second kind. The integration over the arclength is performed numerically using Gauss–Legendre quadrature formulae. When the integrand is singular, the logarithmic singularity is subtracted and an appropriate quadrature scheme is utilized to complete the integration. For details concerning these aspects the reader is referred to the work of Taib (1985). Having evaluated the fluid velocity at S equations (11) and (12) are integrated in time using a second-order Runge–Kutta scheme.

The significant new feature of the results presented here is the computation of non-spherical bubble rebound, caused by the non-condensible bubble contents. The moment of rebound is characterized by very high fluid acceleration, as the direction of the bubble surface motion changes over a very short period of time. In order to capture this fast motion we employ a variable time step δt, chosen as

$$\delta t = \frac{\Delta\phi}{\max_S(\tfrac{1}{2}|\nabla\phi|^2 + \alpha(V_0/V)^\lambda + \delta^2|z-z_0| + 1)}, \tag{14}$$

where $\Delta\phi$ is some constant. With this definition the change in ϕ at each node is bounded above by $\Delta\phi$ over the interval δt. This formula, with the maximum

evaluated over all the nodes defining the bubble surface, possesses the necessary features to enable us to capture bubble rebound with the computational effort somewhat optimized. When the fluid motion is fast the time step is reduced. Furthermore, when the bubble is contracted and $V_0/V \sim 1$, then irrespective of the value of $|\nabla\phi|$ the expression (14) yields very small time steps due to the largeness of α and this allows the rebound of the bubble to be numerically captured. For the computations presented here, $\Delta\phi$ was chosen to be 0.05 although values up to 0.08 give acceptable results.

During the early attempts to compute the rebound of non-spherical bubbles it was found that a sawtooth-type instability developed in the bubble shape in that region where the jet was about to form. As an initial attempt to overcome this difficulty the mesh was redefined after every time step so that the nodes were evenly spaced with respect to the arclength. This allowed the computation to proceed to a slightly greater time but did not prevent the development and rapid growth of this instability. Thus a smoothing scheme is employed and that chosen is the 5-point formula first used by Longuet-Higgins & Cokelet (1976) in their study of steep surface waves on water. The smoothing formula is applied every 5–20 iterations, this application only being essential when attempting to numerically capture rebound.

To ensure that the application of smoothing does not alter the physics embodied in the mathematical model, the changes in kinetic energy, Kelvin impulse and bubble volume brought about by application of smoothing were evaluated. For a typical computation (that considered in §5), during the time until the jet begins to form the relative changes per smoothing operation in kinetic energy, Kelvin impulse and volume are respectively less than 7×10^{-6}, 2×10^{-5} and 2×10^{-5}. This period constitutes $\approx 97\%$ of the bubble lifetime. When the jet forms these changes are respectively less than 7×10^{-4}, 5×10^{-4} and 1×10^{-3} per smoothing operation. Since only about 200 iterations are required to compute the whole motion the smoothing operation is seen to conserve energy, momentum and mass to a high level of precision. Hence we are confident that smoothing does not alter the physics underlying the mathematical description.

4. The Kelvin impulse

The concept of the Kelvin impulse has been utilized to interpret the behaviour of bubbles (Benjamin & Ellis 1966) and predict features of their motion (Blake & Cerone 1982; Blake *et al.* 1986, 1987). The Kelvin impulse of a bubble is defined as

$$\boldsymbol{I} = \rho \oint_S \phi \boldsymbol{n}\, \mathrm{d}S, \tag{15}$$

and corresponds to the impulsive force that would have to be applied over the surface of the bubble to generate the observed flow field from rest. In the context of the deformed, jet-pierced-bubble characteristic of cavity collapse, the Kelvin impulse and jet direction should be closely correlated. It is this postulate that has been the basis for the work of Blake and co-workers (Blake & Cerone 1982; Blake *et al.* 1986, 1987; Blake 1988) in which an approximate expression for the Kelvin impulse at the end of the bubble lifetime is obtained and proposed as giving an indication of the direction of the jet.

The impulse changes in response to the action of external forces, expressed as

$$\mathrm{d}\boldsymbol{I}/\mathrm{d}t = \boldsymbol{F}, \tag{16}$$

and this relationship is analogous to that between the momentum of a particle and the force acting on it. For flows in infinite domains (Blake & Cerone 1982)

$$\boldsymbol{F} = \rho \int_{\Sigma_b} \left[\phi \frac{\partial}{\partial n} (\nabla \phi) - \tfrac{1}{2} |\nabla \phi|^2 \boldsymbol{n} \right] \mathrm{d}S + \rho g V \boldsymbol{e}_z, \tag{17}$$

where Σ_b denotes the boundaries of the flow domain, excluding the bubble surface. The first term represents the Bjerknes force exerted upon the bubble by the boundaries and the second term is the buoyancy force. By approximating the potential at the boundary Σ_b using source-like terms, and using the Rayleigh bubble solution to approximate the strength of the source, the force $\boldsymbol{F}$ may be determined and integration of (16) over the lifetime of the bubble yields an approximation to the impulse at the time of collapse. For motion above a rigid boundary this value is (Blake 1988)

$$I(T_c) \approx (2\sqrt{6\pi}/9\gamma^2)[2\gamma^2\delta^2 B(\tfrac{11}{6}, \tfrac{1}{2}) - B(\tfrac{7}{6}, \tfrac{3}{2})], \tag{18}$$

where T_c is the lifetime of the bubble and B is the beta function (Abramowitz & Stegun 1965). The impulse is scaled with respect to $R_m^3(\rho \Delta p)^{\frac{1}{2}}$.

The interesting feature of (18) is the existence of a null impulse state given by

$$\gamma\delta = (B(\tfrac{7}{6}, \tfrac{3}{2})/2B(\tfrac{11}{6}, \tfrac{1}{2}))^{\frac{1}{2}} = 0.442, \tag{19}$$

for which physical parameters γ and δ the final impulse is approximately zero. It is at this state that the competing Bjerknes and buoyancy forces are approximately equal in their action. Since the Kelvin impulse is related to jetting phenomena, it is found in the case of cavitation motion that jetting is suppressed in the neighbourhood of the null impulse state and the bubble retains much of its spherical character as it collapses (Blake *et al.* 1986).

This last observation is significant in view of the aims of this investigation. Previous studies of underwater explosion phenomena using a boundary-integral method (Chahine & Perdue 1988; Wilkerson 1989) have shown jets forming and completely penetrating the bubble upon the first collapse, with no qualitative evidence that the non-condensible bubble contents act to resist this. However, we propose that for collapse in the neighbourhood of the null impulse state, jetting will be suppressed sufficiently that the bubble may rebound prior to complete penetration by the jet. Thus the null impulse state will form an important part of our investigation.

5. Collapse of non-spherical explosion bubbles

Consider first a typical example of explosion-bubble motion. The motion commences at $\gamma = -2.0$, the negative value indicating motion below the boundary at $z = 0$. The buoyancy parameter is $\delta = 0$ so the only asymmetry in the flow field is due to the presence of the rigid boundary. The strength parameter is $\alpha = 100$ with the corresponding initial radius equal to 0.1651. The bubble shapes at various times throughout the growth and collapse are shown in figure 1. We note that to a very good level of approximation the bubble remains spherical in shape as it expands and also during the early stages of the collapse. As the collapse proceeds the rear side of the bubble becomes noticeably flattened and this perturbation from spherical shape grows rapidly to form the high-speed liquid jet that threads the bubble. The computation cannot proceed beyond the time that the jet impacts upon the far side of the bubble. If we consider that the flattening of the rear of the bubble denotes the

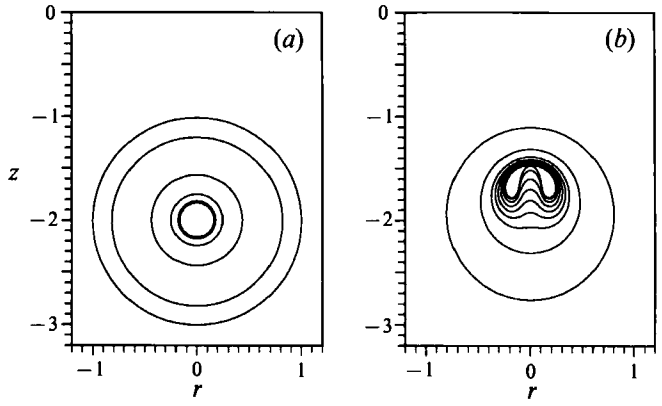

FIGURE 1. Successive bubble shapes for the growth and collapse of a bubble characterized by $\gamma = -2.0$, $\delta = 0$, $\alpha = 100$. The times corresponding to successive profiles are: (*a*) growth phase: 0 (innermost), 0.0082, 0.0237, 0.0860, 0.4108, 1.0692 (outermost); (*b*) collapse phase: 1.7213 (outermost), 2.0197, 2.0719, 2.0878, 2.0984, 2.1076, 2.1158, 2.1231, 2.1269 (innermost).

beginning of jet formation, then inspection of the times corresponding to the profiles shown in figure 1 indicates that the jet forms and completely penetrates the bubble in about 2.5% of the bubble lifetime.

We can consider the mechanism by which the jet is formed in a number of ways. In this case of motion in the neighbourhood of a rigid boundary, upon collapse fluid may be drawn preferentially from the side of the bubble furthermost from the rigid boundary. The increased mobility of the flow from this region causes that part of the bubble surface to collapse more quickly than other parts and form the jet. We consider the mechanism in an alternative manner after computing the pressure field in the fluid by making use of the Bernoulli equation, as has been done previously by Blake *et al.* (1986, 1987). The pressure field in the fluid around the bubble at the times $t = 2.0197$ and 2.1230 is shown in figure 2. At $t = 2.0197$ (figure 2*a*) the bubble is approximately spherical, the pressure inside the bubble is 1.08 and the computed pressure field is typical of that associated with an accelerating sphere. There is a peak of pressure located behind the bubble, with respect to the direction of centroid acceleration. As the bubble accelerates this peak value increases and drives the jet into the bubble. This is indicated in figure 2(*b*) where at $t = 2.1230$ the jet has pierced the bubble with the peak of pressure continuing to drive the fluid in the jet. The pressure within the bubble at this time is 47.63. Thus we can say that for motion in the neighbourhood of a rigid boundary the Bjerknes attraction of the boundary causes the bubble to accelerate towards it upon collapse, with the resultant peak of pressure that develops behind the bubble being the agent that drives the jet into the bubble. This latter view of the cause of jet formation is particularly useful when considering bubble collapse due to buoyancy forces alone. Upon collapse the reducing added mass of the bubble causes it to accelerate upwards causing the formation and rapid intensification of the pressure maximum behind the bubble, which is sufficient to drive a jet into the bubble.

In this example the behaviour of the bubble appears as documented for the collapse of cavitation bubbles, with no qualitative evidence suggesting that the high pressure developed within the bubble as the volume decreases acts to arrest the formation of the jet. We have postulated that in the neighbourhood of the null impulse state the bubble may rebound before jet penetration is complete. We

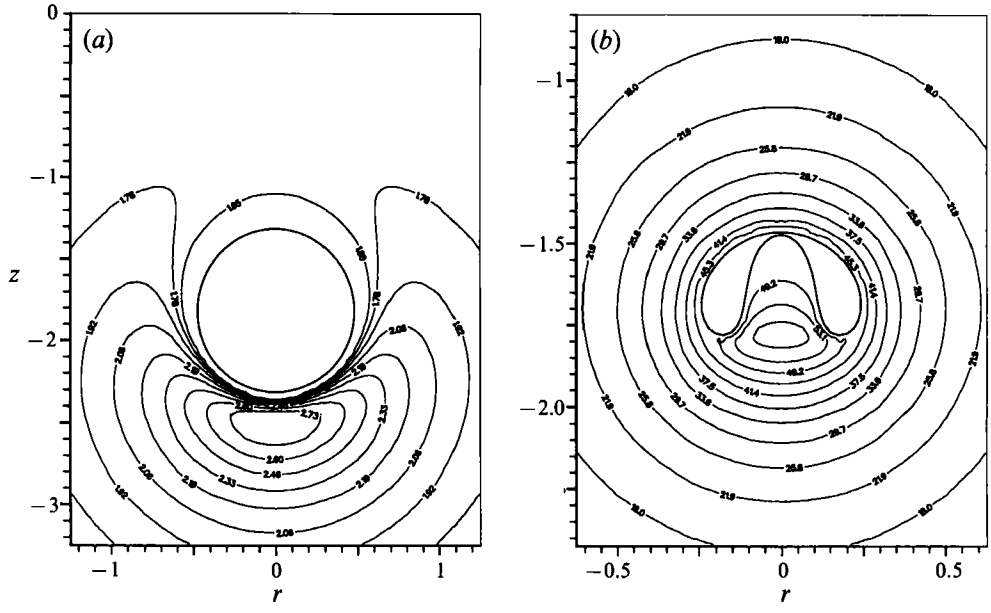

FIGURE 2. The pressure field in the fluid computed for the motion illustrated in figure 1 at times (*a*) 2.0197 and (*b*) 2.1230.

proceed to investigate this matter by considering various regions of the physical parameter space.

6. Variation of the buoyancy parameter

We investigate that subset of the physical parameter space characterized by constant values of $|\gamma|$ and α. We consider motion above and below a rigid boundary and choose $\gamma = \pm 1.5$ with $\alpha = 100$. Our aim is twofold. In the first instance, for $\gamma = 1.5$ the values of the buoyancy parameter chosen lie between 0 and 0.35 and this region of the parameter space includes the null impulse state, in which neighbourhood we expect non-spherical bubble rebound to occur. Secondly, for motion below and above a rigid boundary the buoyancy and Bjerknes forces will respectively act together and in opposition. It is of interest to investigate the features of the collapse that vary as these forces vary and determine qualitative principles describing this variation.

The primary result is shown in figure 3, where the computed bubble shape is shown at the time when the jet completely penetrates the bubble, or when the bubble achieves a minimum of volume. The time at which it occurs is given below each bubble shape. These results bear some similarity to the final shapes of cavitation bubbles computed by Blake *et al.* (1986). Consider the upper sequence, characterized by $\gamma = -1.5$, as δ decreases from 0.35 to 0. In this case the buoyancy and Bjerknes forces are similarly directed. As δ decreases, the time at which jet penetration is complete generally tends to decrease but this variation is negligible compared to the lifetime of the bubble. It appears that the lifetime of the bubble depends little upon the buoyancy parameter. As δ decreases, the breadth of the jet decreases, as does the volume of the bubble at the end of its life. To assist in the interpretation of this behaviour we have computed the velocity of that point on the bubble surface that evolves into the jet tip, as a function of time, and we call this the jet velocity. Its

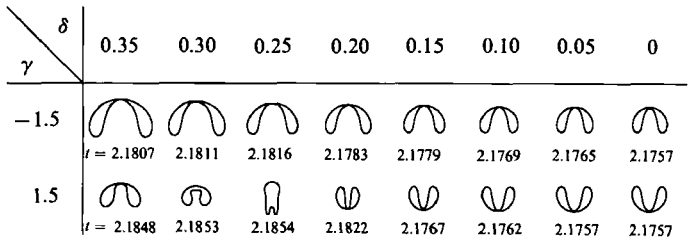

FIGURE 3. Bubble shapes at the time of jet penetration, or minimum volume, for a range of buoyancy parameters. The motion begins at a distance of 1.5 above ($\gamma = 1.5$) and below ($\gamma = -1.5$) a rigid boundary. The strength parameter is $\alpha = 100$.

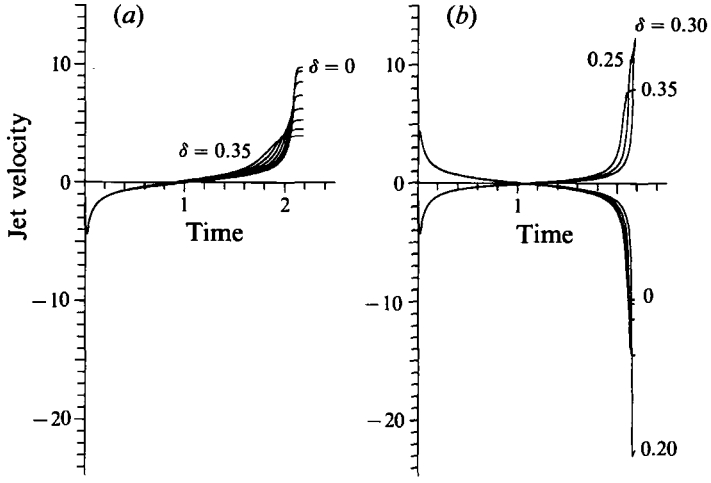

FIGURE 4. Jet tip velocity as a function of time for each of the motions considered in figure 3. The frames display this velocity for the cases (*a*) $\gamma = -1.5$ and (*b*) $\gamma = 1.5$. In cases where each curve is not individually labelled there is a systematic trend in the corresponding value of δ, between the extremes noted.

variation for the bubbles currently under consideration is shown in figure 4 (*a*). The jet velocity data reveal a number of interesting features. In all cases the departure from spherical shape is signified by a rise in the velocity of that part of the surface where the jet will form, above the value expected for a spherical bubble. The larger the value of δ the sooner this occurs. This is due to the large value of the buoyancy force coupling with the Bjerknes force to accelerate the bubble more rapidly as it collapses, causing a premature departure from spherical shape. If we consider the buoyancy and Bjerknes forces as agents perturbing the spherical shape then the magnitude of the perturbation increases with δ, leading to premature collapse and a larger jet. Accompanying this behaviour is a final jet velocity that increases with decreasing δ and a final Kelvin impulse that increases with δ.

There appears to be some inverse relationship between the jet velocity and the breadth of the jet, although these quantities are not well defined. This qualitative inverse relationship bears a remarkable similarity to the inverse relationship between mass and velocity for a particle of given momentum in rigid-particle mechanics. This is not unexpected in view of the analogy between particle momentum and the Kelvin impulse. We remark, however, that the final values of the impulse are different for each of these examples and this must impose some limit upon the extent of the

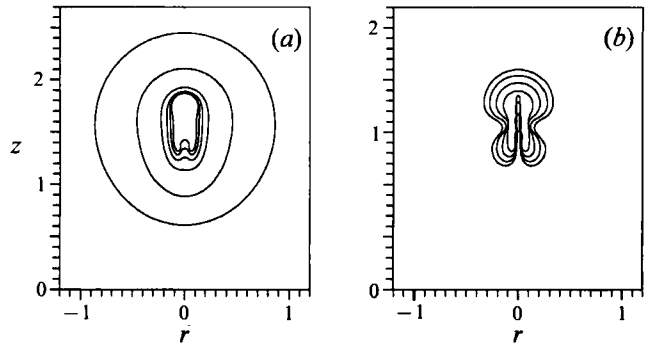

FIGURE 5. Successive bubble shapes for (*a*) the collapse and (*b*) rebound of a bubble characterized by $\gamma = 1.5$, $\delta = 0.25$, $\alpha = 100$.

analogy. We could perhaps proceed in quantifying this analogy by introducing mathematically precise quantities associated with the jet width and jet velocity and investigating their relationship with the Kelvin impulse. These quantities may be appropriate averages over the volume of the jet but it is not obvious how we should proceed in such an endeavour. We leave such an investigation for later attention.

A further significant feature of the jet velocity *vs.* time data is what we shall refer to as the terminal velocity characteristic. The jet accelerates rapidly shortly after formation, but this acceleration subsequently slows and the jet tip velocity levels to some constant terminal value. That this should occur may be explained in a number of ways. Recall the local maximum of pressure that develops in the fluid behind the bubble, as it accelerates forward upon collapse. This causes the flow into the high-speed jet, but as the flow continues this maximum of pressure is relieved and the pressure gradient between this point and the bubble surface falls. As a consequence the fluid acceleration there falls to zero and the jet tip achieves a terminal velocity. From a global perspective, as the bubble collapses much of the fluid momentum manifests itself in the jet. Since only a finite amount of momentum may be transferred to the jet it cannot continue to accelerate after the transfer of finite momentum has occurred.

Consider now the collection of bubble shapes for motion at $\gamma = 1.5$ as δ ranges between 0 and 0.35 (figure 3). In this case the buoyancy and Bjerknes forces act in opposition and we note the transition in behaviour as δ varies. In the case of small δ, the Bjerknes attraction dominates and the jet is directed towards the boundary. As δ increases, buoyancy assumes dominance and for large δ the jet is directed upwards. A very interesting behaviour occurs at $\delta = 0.25$ where the buoyancy force and Bjerknes force are nearly equal in their effect. This set of physical parameters is in the neighbourhood of the null impulse state; the computed value of the impulse at the time shown is 0.0223. We consider this case in more detail.

The collapse and rebound of an explosion bubble characterized by $\gamma = 1.5$, $\delta = 0.25$, $\alpha = 100$ is shown in figure 5. The bubble remains approximately spherical during the growth phase. Owing to the approximately equal and opposite buoyancy and Bjerknes forces there is little translational motion of the bubble upon collapse, the result being that fluid is preferentially drawn in from the sides leading to an elongation of the bubble along the axis of symmetry. Buoyancy is slightly dominant in this case and the slight upwards acceleration upon collapse leads to the elements of a jet being evident at minimum volume. In this neighbourhood of the null impulse state jetting has been suppressed sufficiently that the bubble rebounds, this phase of

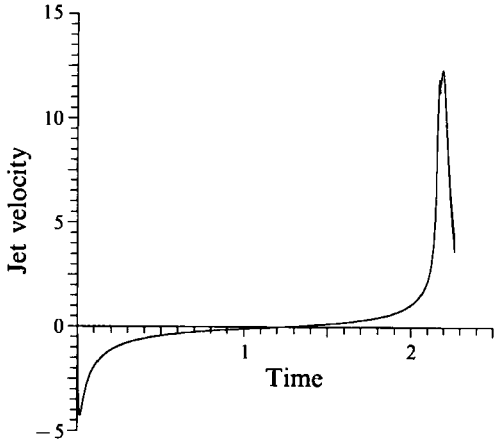

FIGURE 6. Jet tip velocity as a function of time for the motion depicted in figure 5.

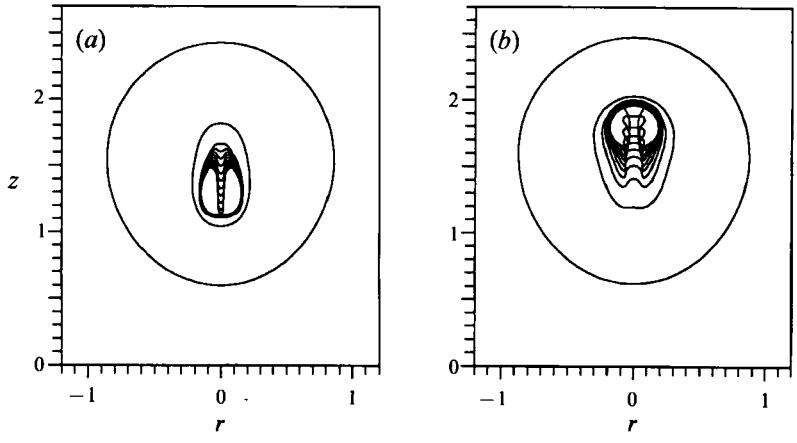

FIGURE 7. Successive bubble shapes for the collapse of bubbles characterized by $\gamma = 1.5$, $\alpha = 100$, and (*a*) $\delta = 0.23$, (*b*) $\delta = 0.27$.

the motion being shown in figure 5(*b*). As the bubble re-expands the jet continues to be driven into the bubble. The inwards radial motion of the fluid, about the centre of the bubble, is arrested at rebound but causes what we shall call upper and lower lobes of the bubble to develop. As a result of this inwards flow, the high pressure within the bubble at minimum volume preferentially causes the rapid re-expansion of the upper and lower parts of the bubble leading to the observed lobe structure. The jet tip velocity as a function of time for this example is shown in figure 6. The opposite coupling of buoyancy and Bjerknes forces gives rise to a very small initial perturbation in the bubble shape resulting in delayed jet formation and a thin jet. Accompanying this small amount of mass in the jet is a very high peak jet velocity achieved at around minimum volume. As the bubble re-expands, the jet velocity falls, although the jet continues to travel through the bubble. The rebound causes the bulk of the fluid surrounding the bubble to flow outwards, this outflow reducing the rate of flow into the jet, causing it to decelerate.

Consider the behaviour for values of the buoyancy parameter of about 0.25. The collapse of an explosion bubble characterized by $\gamma = 1.5$, $\delta = 0.23$, $\alpha = 100$ is shown in figure 7(*a*). In this example the Bjerknes force slightly dominates the buoyancy force and the jet is directed towards the boundary. As the bubble collapses we note

the elongation along the axis of symmetry. Since the buoyancy and Bjerknes forces act in opposition, jet formation is delayed and the jet that forms contains a small amount of mass. Accompanying this is a very high jet velocity as evident from inspection of figure 4. We comment that the bubble achieves a minimum volume just prior to the time that the jet completely penetrates the bubble. The collapse of an explosion bubble characterized by $\gamma = 1.5$, $\delta = 0.27$, $\alpha = 100$ is shown in figure 7(*b*). This example exhibits many of the features discussed above although in this case the buoyancy force is slightly dominant, with the jet that forms directed upwards. The interesting feature here is the pluming of the jet. As the jet is driven into the bubble the top broadens so that its radius there is greater than at its base. This appears to be a feature of explosion-bubble collapse in the neighbourhood of the null impulse state, in the case where buoyancy is slightly dominant. A similar behaviour has been observed experimentally for the motion of two-dimensional bubbles of constant volume rising slowly under the action of buoyancy forces alone (Walters & Davidson 1962) and computations of this motion are in good agreement (Baker & Moore 1989; Lundgren & Mansour 1991).

We remark that trends in the bubble behaviour upon collapse follow the general principles discussed for the case where buoyancy and the Bjerknes attraction act together. For a larger resultant perturbing effect jet formation is initiated early and a larger amount of mass is contained in the jet. This is accompanied by a smaller final jet velocity. About the null impulse state the initial perturbation in the bubble shape is small with narrow jets being formed and characterized by the highest speeds. In the neighbourhood of the null impulse state the non-spherical bubble has been shown to rebound. If we compare cases characterized by the same buoyancy parameter then there is a greater absolute value of the final Kelvin impulse in the case where the two forces act together, with a broader jet and small jet velocity, in accord with our general principles. In the case where the forces are in opposition we have a smaller initial perturbing effect, giving rise to narrower jets of higher velocity. These examples for $\gamma = 1.5$ demonstrate the small influence that the buoyancy parameter has upon the lifetime of the bubble, the variation over the range of δ considered here being insignificant compared with the lifetime of the bubble and of the order of the computational error.

7. Variation of the distance of inception from a rigid boundary

Consider now the varying behaviour of a deforming explosion bubble as the distance of inception from a rigid boundary is varied. The bubble shapes at the time of complete jet penetration, or minimum volume, are shown in figure 8 over a range of values of γ between 1 and ∞, for a strength parameter $\alpha = 100$ and buoyancy parameter of $\delta = 0.20$. Motion is considered both above and below a rigid boundary to display both the positive and negative coupling of the buoyancy and Bjerknes forces. For each of the bubbles depicted in this figure the jet tip velocity is shown as a function of time in figure 9.

As for the results presented for varying δ we note similar trends in the changing character of the collapse with varying γ. The larger the resultant perturbing force, the broader the jet and smaller the final jet tip velocity. For motions characterized by the same absolute value of the physical parameters, in the case of motion above the boundary the perturbing force is smaller due to the opposite coupling of the buoyancy and Bjerknes forces, giving rise to a smaller jet with higher velocity. The terminal velocity feature is evident. For motion above the boundary we note the

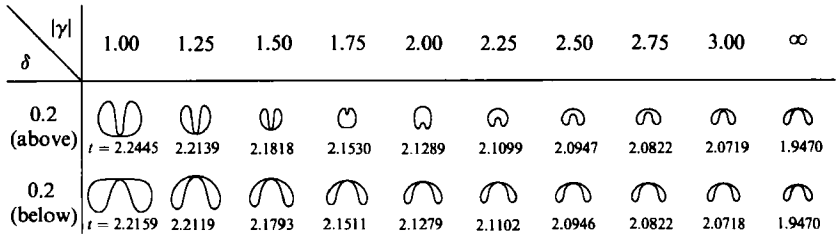

FIGURE 8. Bubble shapes at the time of jet penetration, or minimum volume, for a range of distances of inception from a rigid boundary. The buoyancy parameter is $\delta = 0.2$ and the strength parameter is $\alpha = 100$. Motion is considered both above and below the boundary.

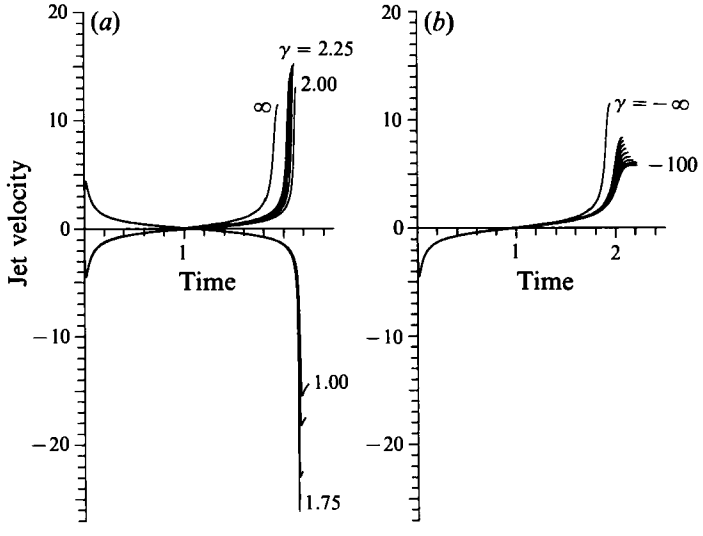

FIGURE 9. Jet tip velocity as a function of time for each of the motions considered in figure 8. The frames display this velocity for motion (*a*) above and (*b*) below a rigid boundary. In cases where each curve is not individually labelled there is a systematic trend in the corresponding value of γ, between the extremes noted.

transition from jet formation directed upwards to jet formation directed downwards as the relative strengths of the buoyancy and Bjerknes forces change. Consider the collapse and rebound of a bubble about the null impulse state. This is shown in figure 10 for an explosion bubble characterized by $\gamma = 1.85$, $\delta = 0.20$, $\alpha = 100$. The significant features are much as for the rebounding bubble shown in the previous section, including the formation of upper and lower lobes. The rapid re-expansion of the lobes leads to a ring of very high surface curvature about the centre of the bubble. The thin jet also exhibits very high curvature during the later stages of the bubble's life. Beyond this time the computational scheme cannot proceed. In reality surface tension and pressure fluctuations within the bubble contents will break up this high-curvature surface. Especially significant in the case of explosion-bubble motion is the temperature of the bubble contents which may lead to a phase transition at the bubble surface and provide a further mechanism for the breakup of high-curvature regions of the bubble surface.

In contrast to the negligible variation of lifetime with δ noted in §6, here a systematic trend is evident in the lifetime of the bubble over the range of γ. We can

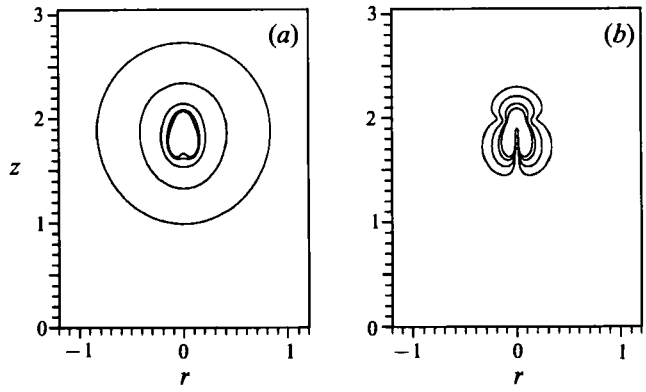

FIGURE 10. Successive bubble shapes for (*a*) the collapse and (*b*) rebound of a bubble characterized by $\gamma = 1.85$, $\delta = 0.2$, $\alpha = 100$.

explain this behaviour in terms of the mobility of the fluid. The ease with which the fluid between the bubble and the boundary may be displaced is dependent upon the geometry of the flow field. In this example the geometry is characterized by γ, the difficulty in displacing fluid during both expansion and collapse increasing with the proximity of the boundary. Hence the lifetime increases as γ decreases and is quite independent of δ, although the early migration due to buoyancy forces may have some minor influence.

8. Discussion and conclusions

The strength parameter gives some measure of the amplitude of the radial oscillations of a bubble. The smaller its value, the smaller the amplitude of the oscillations and consequently the radial fluid velocities upon collapse are smaller. Thus in the regime of small strength parameters the high pressure created within the bubble upon its contraction may be sufficient to delay the formation of the jet, allowing the bubble to rebound in connected form. We consider an example of bubble motion characterized by a small value of the strength parameter. The collapse and rebound of a bubble characterized by $\gamma = \infty$, $\delta = 0.15$ and $\alpha = 10$ is shown in figure 11 and the vertical scale is arbitrary. The initial radius is 0.3804. Since it is the reducing added mass of the bubble upon collapse that gives rise to the rapid acceleration phase that precipitates jet formation, the relative smallness of the change in added mass over the oscillation period of the bubble in this example gives rise to a smaller upwards acceleration upon collapse, so that only the elements of a jet are evident at rebound. As the bubble rebounds the jet continues to travel into the bubble, the reducing pressure within the bubble assisting in this endeavour. Despite the formation of a jet, the bubble retains much of its spherical character.

We consider here a number of other examples of bubble motion that are of interest and remark upon some of the implications of the results presented in this paper. We have postulated that in the neighbourhood of the null impulse state non-spherical bubbles should rebound. The results presented in this paper have demonstrated this but only for a strength parameter of 100. The behaviour that occurs in the neighbourhood of the null impulse state for increased strength parameters is of interest. We consider two further examples for a strength parameter of 1000. The example shown in figure 12(*a*) is of the collapse of a bubble characterized by $\gamma = 2.0$

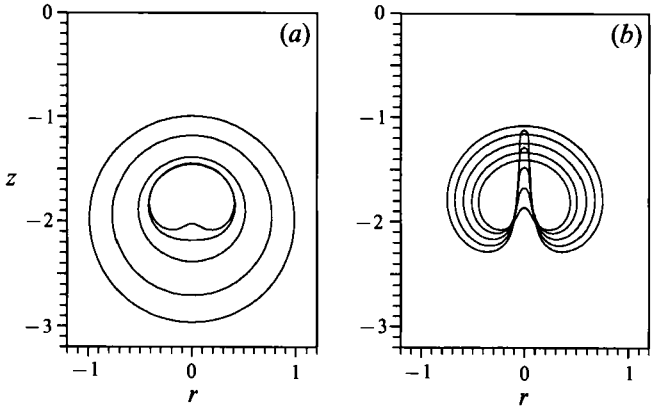

FIGURE 11. Successive bubble shapes for the collapse and rebound of a bubble characterized by $\gamma = \infty$, $\delta = 0.15$, $\alpha = 10$.

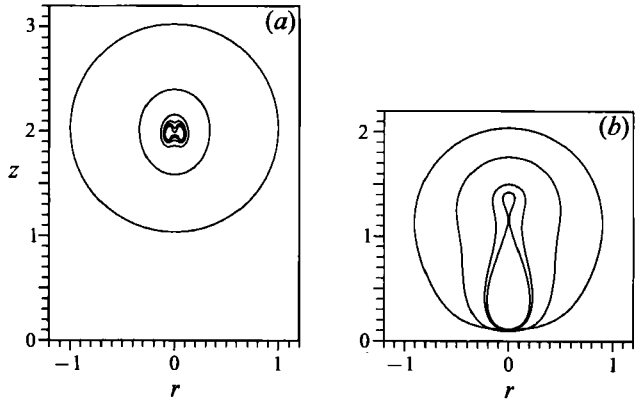

FIGURE 12. Successive bubble shapes for the collapse of bubbles characterized by $\alpha = 1000$ and (*a*) $\gamma = 2.0$, $\delta = 0.1948$, and (*b*) $\gamma = 1.0$, $\delta = 0.33$.

and $\delta = 0.1948$, with this value of δ determined so that the bubble is close to the null impulse state. The initial radius is 0.0748. The significant feature is that both upper and lower jets have formed in this case. Note that the lower jet is broader than the upper jet. In this case the fluid speed upon collapse is so high that both jets penetrate the bubble sufficiently that the bubble does not rebound in connected form.

Consider the further example characterized by $\gamma = 1$ and $\delta = 0.33$, as shown in figure 12 (*b*), with the value of δ again determined such that the bubble is near the null impulse state. The behaviour in this case is very different. Owing to the close proximity of the rigid boundary, fluid cannot be easily drawn in from near to the rigid boundary and jet formation at the base of the bubble is resisted. As a consequence fluid is preferentially drawn in radially leading to the formation of upper and lower bubble lobes. Although the fluid is more mobile away from the rigid boundary, the formation of a jet here would lead to a significant value of the impulse, but this cannot occur in this neighbourhood of the null impulse state. After the last time shown in this figure the bubble will split to form two bubbles and these bubbles may possibly be threaded by jets that originate from the contact point. The formation of such a lobe structure upon collapse has been experimentally observed

for motion near a compliant surface (Gibson & Blake 1982) and between parallel rigid boundaries (Chahine 1982), in the case where the bubble is in the neighbourhood of the null impulse state.

The results for rebounding bubbles, although computed using an incompressible description, have implications for the emission of pressure pulses upon rebound. It has been proposed (Shiffman & Friedman 1944) that such emission will be enhanced in the case where the buoyancy and the Bjerknes forces are almost equal and opposite. The results of this investigation have demonstrated that in this case the bubble can preserve much of its spherical character about the time of rebound. In the bulk of cases jet penetration occurs before the bubble rebounds, with kinetic energy then becoming bound in the vortex ring structure which then evolves. In the case of motion in the neighbourhood of the null impulse state, however, for not too large values of the strength parameter, it is evident that the bubble rebounds before the jet has completely penetrated it. We might suppose that in this case the emission of acoustic energy at rebound will be enhanced, but such a speculation must be investigated either experimentally or computationally by a solution of the equations of compressible flow. Such an investigation has practical implications for underwater explosions occurring near the ocean floor.

We would like to thank Professor J. R. Blake for commenting on this manuscript and for helpful discussions throughout the course of this work. This work was partially supported by the Australian Research Council.

REFERENCES

ABRAMOWITZ, M. & STEGUN, I. A. 1965 *Handbook of Mathematical Functions*, Dover.

BAKER, G. R. & MOORE, D. W. 1989 The rise and distortion of a two-dimensional gas bubble in an inviscid liquid. *Phys. Fluids* A **1**, 1451–1459.

BENJAMIN, T. B. & ELLIS, A. T. 1966 The collapse of cavitation bubbles and the pressures thereby produced against solid boundaries. *Phil. Trans. R. Soc. Lond.* A **260**, 221–240.

BLAKE, J. R. 1988 The Kelvin impulse: Application to cavitation bubble dynamics. *J. Austral. Math. Soc.* B **30**, 127–146.

BLAKE, J. R. & CERONE, P. 1982 A note on the impulse due to a vapour bubble near a boundary. *J. Austral. Math. Soc.* B **23**, 383–393.

BLAKE, J. R., TAIB, B. B. & DOHERTY, G. 1986 Transient cavities near boundaries. Part 1. Rigid boundary. *J. Fluid Mech.* **170**, 479–497.

BLAKE, J. R., TAIB, B. B. & DOHERTY, G. 1987 Transient cavities near boundaries. Part 2. Free surface. *J. Fluid Mech.* **181**, 197–212.

CHAHINE, G. L. 1982 Experimental and asymptotic study of non-spherical bubble collapse. *Appl. Sci. Res.* **38**, 187–197.

CHAHINE, G. L. 1990 Numerical modelling of the dynamic behaviour of bubbles in non-uniform flow fields. In *Proc. ASME 1990 Symp. on Numerical Methods for Multiphase Flows, Toronto.*

CHAHINE, G. L. & PERDUE, T. O. 1988 Simulation of the three-dimensional behaviour of an unsteady large bubble near a structure. In *Proc. 3rd Intl Colloq. on Drops and Bubbles, Monterey, California.*

GIBSON, D. C. & BLAKE, J. R. 1982 The growth and collapse of bubbles near deformable surfaces. *Appl. Sci. Res.* **38**, 215–224.

GUERRI, L., LUCCA, G. & PROSPERETTI, A. 1981 A numerical method for the dynamics of non-spherical cavitation bubbles. In *Proc. 2nd Intl Colloq. on Drops and Bubbles, Monterey, California. JPL Publication* 82-7, pp. 175–181.

KUCERA, A. 1992 A boundary integral method applied to the growth and collapse of bubbles near a rigid boundary. *J. Comput. Phys.* (submitted).

LAUTERBORN, W. & BOLLE, H. 1975 Experimental investigations of cavitation bubble collapse in the neighbourhood of a solid boundary. *J. Fluid Mech.* **72**, 391–399.

LONGUET-HIGGINS, M. S. & COKELET, E. D. 1976 The deformation of steep surface waves on water. I. A numerical method of computation. *Proc. R. Soc. Lond.* A **350**, 1–26.

LUNDGREN, T. S. & MANSOUR, N. N. 1991 Vortex ring bubbles. *J. Fluid Mech.* **224**, 177–196.

RAYLEIGH, LORD 1917 On the pressure developed in a liquid during the collapse of a spherical void. *Phil. Mag.* **34**, 94–98.

SHIFFMAN, M. & FRIEDMAN, B. 1944 On the best location of a mine near the sea bed. In *Underwater Explosion Research*, Vol. II. Office of Naval Research, Washington, DC.

TAIB, B. B. 1985 Boundary integral methods applied to cavitation bubble dynamics. Ph.D. thesis, University of Wollongong, Australia.

TOMITA, Y. & SHIMA, A. 1986 Mechanisms of impulsive pressure generation and damage pit formation by bubble collapse. *J. Fluid Mech.* **169**, 535–564.

VOGEL, A., LAUTERBORN, W. & TIMM, R. 1989 Optical and acoustic investigations of the dynamics of laser-produced cavitation bubbles near a solid boundary. *J. Fluid Mech.* **206**, 299–338.

WALTERS, J. K. & DAVIDSON, J. F. 1962 The initial motion of a gas bubble formed in an inviscid liquid. Part 1. The two-dimensional bubble. *J. Fluid Mech.* **12**, 408–417.

WILKERSON, S. 1989 Boundary integral technique for explosion bubble collapse analysis. *ASME Energy-Sources Technol. Conference and Exhibition, Houston, Texas.*